

Title	Study on residual OH content in low-temperature Si oxide films after in situ post-deposition heating (PDH)
Author(s)	Horita, Susumu; Pu, Di
Citation	Japanese Journal of Applied Physics, 63(01SP12): 1-9
Issue Date	2023-12-20
Type	Journal Article
Text version	publisher
URL	<a href="http://hdl.handle.net/10119/18795">http://hdl.handle.net/10119/18795</a>
Rights	Copyright (c) 2023 Authors. Susumu Horita, Di Pu. Japanese Journal of Applied Physics 63, 01SP12 (2024). This is an Open Access article distributed under the terms of Creative Commons Licence CC-BY [ <a href="https://creativecommons.org/licenses/by/4.0/">https://creativecommons.org/licenses/by/4.0/</a> ]. Original publication is available on IOP Science via <a href="https://doi.org/10.35848/1347-4065/acf477">https://doi.org/10.35848/1347-4065/acf477</a> .
Description	



# Study on residual OH content in low-temperature Si oxide films after in situ post-deposition heating (PDH)

Susumu Horita\* and Di Pu

Japan Advanced Institute of Science &amp; Technology, 1-1 Asahidai, Ishikawa, 923-1292, Japan

\*E-mail: [horita@jaist.ac.jp](mailto:horita@jaist.ac.jp)

Received July 17, 2023; revised August 20, 2023; accepted August 27, 2023; published online December 20, 2023

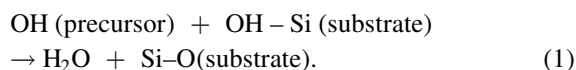
We investigated the post-deposition heating (PDH) effect on OH content in SiO<sub>x</sub> films deposited by atmospheric-pressure CVD using a deposition source of silicone oil (SO) with O<sub>3</sub> and TCE vapor at a temperature  $T_d$  of 180 °C–250 °C. The PDH is performed in situ for 5 min in the deposition chamber just after film deposition without any supply of SO, where the heating temperature is the same as  $T_d$ . The OH content in the films deposited normally decreases with increasing  $T_d$ . In contrast, those with PDH decrease with decreasing  $T_d$  from 220 °C, and, at  $T_d = 190$  °C, a minimum OH content can be obtained. This means that lower OH content remains at a lower deposition temperature. The PDH effect on OH reduction can be explained by easily reconstructible structure of SiO<sub>x</sub> films deposited at low temperature. Furthermore, we discuss the mechanism of the PDH effect from other points of view. © 2023 The Author(s). Published on behalf of The Japan Society of Applied Physics by IOP Publishing Ltd

## 1. Introduction

Low-temperature deposition of silicon oxide (SiO<sub>x</sub>) films is required for the fabrication of not only thin-film transistors on non-heat-resistant substrates<sup>1</sup> but also interlayer dielectrics in size-minimizing ICs to suppress the disconnection of the interconnect metal, the redistribution of the dopant, and defect generation in the fabricated underlayer.<sup>2</sup> For low-temperature deposition, plasma-enhanced CVD (PECVD) has been widely used in practice,<sup>1,3–6</sup> which requires an expensive system consisting of vacuum equipment and high power supply. In addition, tetraethylorthosilicate [TEOS; Si(OC<sub>2</sub>H<sub>5</sub>)<sub>4</sub>] vapor is commonly used as a deposition gas source.<sup>3–5</sup> On the other hand, we previously reported on the low-temperature deposition of SiO<sub>x</sub> films using silicone oil {SO: dimethylpoly-siloxane (CH<sub>3</sub>)<sub>3</sub>SiO[(CH<sub>3</sub>)<sub>2</sub>SiO]<sub>10</sub>Si(CH<sub>3</sub>)<sub>3</sub>} vapor as a deposition source and ozone (O<sub>3</sub>) gas at temperatures of 200 °C–350 °C at atmospheric pressure without vacuum or pumping systems.<sup>7,8</sup> SO has advantages over TEOS; the price per unit volume of SO is lower than that of TEOS by about one order, and SO is not only markedly thermally stable, but also a safe material, whereas TEOS is toxic especially to the human eye and throat.<sup>9</sup>

In addition, in order to increase the rate (less than 5 nm min<sup>-1</sup>) of SiO<sub>x</sub> film deposition, by changing SO to decamethylcyclopenta-siloxane, C<sub>10</sub>H<sub>30</sub>O<sub>5</sub>Si<sub>5</sub>, we have reported that adding some amount of trichloroethylene (C<sub>2</sub>HCl<sub>3</sub>; TCE) vapor markedly increases the deposition rate to more than three times that without TCE during deposition in combination with SO and O<sub>3</sub> at deposition temperatures lower than 200 °C.<sup>10</sup> Furthermore, when using TCE, the OH content in the deposited SiO<sub>x</sub> films is much reduced by nearly half of that without it.<sup>11,12</sup>

This increase in the deposition rate and reduction of OH content are caused by TCE-enhanced dehydration reaction between silanols of the precursors and OH bonds terminated at the surface of the substrate or deposited film, i.e.,



TCE may be decomposed into H and C among others due to the highly reactive O<sub>3</sub>, and hydrochloric acid can be formed. Acid added into an organic chemical solution is well known as a catalyst to enhance the dehydration reaction in an organic chemical solution, e.g. the so-called Fischer esterification reaction.<sup>13</sup>

However, using TCE for the SiO<sub>x</sub> film deposition with SO + O<sub>3</sub>, the deposited films still contain a large number of OH bonds, which have been reported to lead to the serious problems of high leakage current and low breakdown voltage.<sup>8,14–16</sup> Generally, low-temperature SiO<sub>x</sub> films prepared by CVD methods with organic silicon sources, such as TEOS, are more likely to contain a large number of OH bonds when no special treatment is carried out, e.g. post-deposition annealing. In fact, it has already been reported that annealing with higher temperature of more than 400 °C makes residual OH bonds vanish from the deposited film and it improves the electrical properties, e.g. lower leakage current and higher breakdown voltage.<sup>8,17,18</sup> However, high-temperature annealing may lose some effectiveness of the low-temperature deposition process. Therefore, in order to reduce the number of residual OH bonds before removing a deposited film from the deposition chamber, we treated a deposited SiO<sub>x</sub> film by in-site post-deposition heating (PDH) and compared the OH content with that of a non-PDH(NPDH)-treated film. In this paper, having reported some results in the previous conference of EM-NANO 2023,<sup>19</sup> we will provide many more results with respect to the PDH process and deeply discuss them. Finally, we suggest an effective technique to produce a lower-temperature deposited SiO<sub>x</sub> film with lower OH content.

## 2. Experimental

Figure 1(a) shows a schematic diagram of the deposition system used in this study. The system has a vertical reactor for atmospheric-pressure (AP) CVD. The details are mentioned in a previous paper.<sup>10</sup> Before setting n-type (111)Si substrates on a stainless-steel holder, they were chemically cleaned in a hot



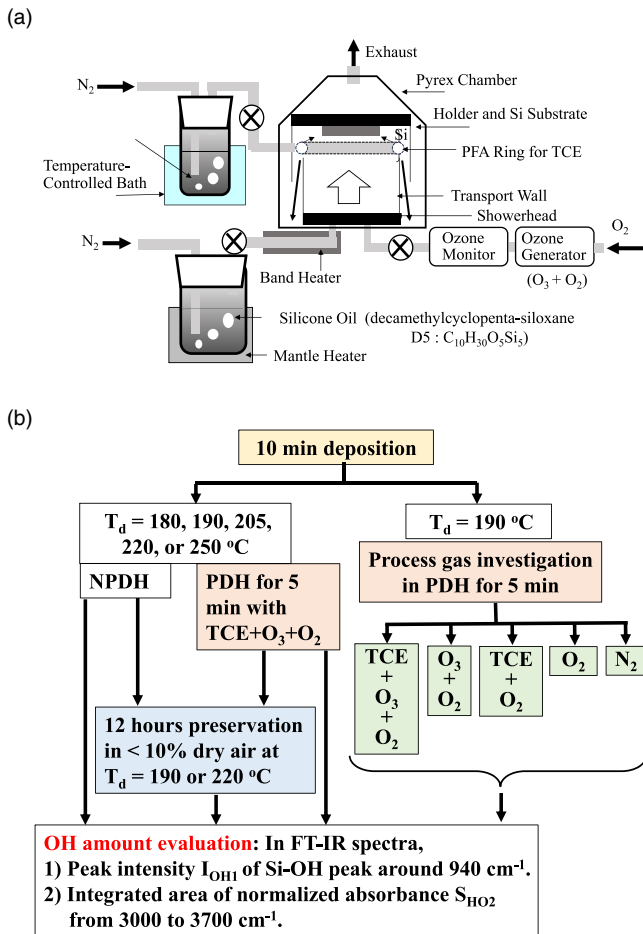


**Fig. 1.** (a) Schematic diagram of the deposition APCVD system used in this study. Deposition chamber and sample holder are made of Pyrex glass and stainless steel, respectively. (b) PDH process flow. Left- and right-hand sides show the normal PDH process and the PDH processes with various process gases, respectively. NPdH is an abbreviation of no post-deposition heating.

acid solution and dipped in a dilute HF solution to remove Si oxide. The SO used was decamethylcyclopenta-siloxane ( $C_{10}H_{30}O_5Si_5$ ) heated to  $50\text{ }^\circ\text{C}$  using a mantle heater, and its vapor was generated by bubbling with  $N_2$  gas. The flow rate of  $N_2$  gas for the SO vapor,  $F_{N_2}(\text{SO})$ , was  $0.2\text{ lmin}$  (liters per minute at  $20\text{ }^\circ\text{C}$ ).  $O_3$  was generated using a silent electric discharge from  $99.9995\%$   $O_2$  gas at a flow rate of  $0.50\text{ lmin}$  and the  $O_3$  concentration was  $\sim 150\text{ g m}^{-3}$ . The  $O_3 + O_2$  mixed gas was introduced into the reaction chamber from the bottom. The TCE vapor was generated by bubbling  $20\text{ }^\circ\text{C}$  TEC solution with  $0.1\text{ lmin}$   $N_2$  gas, and the mixed gas of TCE vapor +  $N_2$  gas was introduced into a PFA tube with a  $1/4$  inch diameter. The mixed gas was blown onto the Si substrates directly through many  $\sim 2\text{ mm-}\phi$  holes made in a PFA tube ring with a diameter of  $\sim 110\text{ mm}$ . The distance between the ring and the sample holder was  $\sim 10\text{ mm}$ .  $SiO_x$  films were deposited for  $10\text{ min}$  at a deposition temperature  $T_d$  of  $180\text{ }^\circ\text{C}$ – $250\text{ }^\circ\text{C}$ . After the deposition, the heating of the sample holder was stopped immediately, and then for the same samples, the supply of SO vapor, TCE vapor and  $O_3 + O_2$  gases was stopped and we immediately flowed pure  $N_2$  gas at  $\sim 2\text{ lmin}$  onto the sample holder. Soon after the holder was cooled down to  $120\text{ }^\circ\text{C}$  from the  $T_d$ , the deposited samples were removed from the deposition chamber. This is called the non-post-deposition-heating

(NPdH) process. The other samples, just after the deposition, were heated in situ for  $5\text{ min}$  at the same  $T_d$  of  $180\text{ }^\circ\text{C}$ – $250\text{ }^\circ\text{C}$  without any supply of SO vapor, as shown in the left-hand side of Fig. 1(b). This is the so-called PDH. The gas used for the PDH process was mainly a mixed gas of TCE(+ $N_2$ ) +  $O_3 + O_2$  or deposition reactant gas without SO vapor. After taking out some samples treated by PDH at  $190\text{ }^\circ\text{C}$  or  $220\text{ }^\circ\text{C}$ , they were preserved in dry air with humidity of less than  $10\%$  for  $12\text{ h}$  at RT. For comparison, some NPdH samples at  $190\text{ }^\circ\text{C}$  or  $220\text{ }^\circ\text{C}$  were also preserved. The preservation was done to investigate the PDH effect on the suppression of increase in OH content. Many researchers have already reported that OH content in low-temperature deposition  $SiO_x$  films increases during preservation in air mainly due to moisture adsorption on the film surface from the preservation atmosphere.<sup>4,20,21</sup> Furthermore, gas of the PDH process was changed to  $O_3 + O_2$ , TCE +  $O_2$ ,  $O_2$  or  $N_2$  to investigate the influence of the process gas on OH content in the deposited films, as shown in the right-hand side of Fig. 1(b). For simplification, the name of each PDH process with a different gas combination is abbreviated to  $P_i$ , as shown in Table I including the NPdH process, where the subscript  $i$  is an integer corresponding to used gaseous species. For example, PDH processes with gases of TCE +  $O_3 + O_2$  and  $O_3 + O_2$  are labeled as  $P_1$  and  $P_2$ , respectively.

The thicknesses  $d$  and refractive indexes  $n$  of the deposited films were measured by ellipsometry using four wavelengths of  $450, 525, 595,$  and  $660\text{ nm}$  from four LEDs (Model FS-1, Film Sense LLC). The molecular structures of the films were analyzed from Fourier transform IR spectroscopy (FT-IR) spectra with a resolution of  $4\text{ cm}^{-1}$  and the acquired spectra were averaged with  $10$  scans. The measured FT-IR spectra were normalized by the highest peak of the Si–O–Si unsymmetric stretching ( $TO_3$ ) vibration mode around  $1065\text{ cm}^{-1}$ , as shown later in Fig. 3(a).<sup>22–24</sup> In order to improve the signal-to-noise ratio, the measured spectra were computed by two runs of a five-point moving average with a parabolic smoothing function. In addition, we took the 1st derivative of the averaged spectra by using the Savitzky–Golay numerical algorithm with the 2nd-order polynomial at  $20$  points to estimate the width of the  $TO_3$  mode peak instead of the FWHM.<sup>25</sup> The difference in wavenumber  $k$  between the 1st derivative maximum and the 1st derivative minimum of the peak is proportional to the FWHM, as mentioned in the Appendix. For the quantitative amount of OH content in the deposited  $SiO_x$  films, we used two characteristic values from the FT-IR spectra. One is an FT-IR peak intensity of normalized absorbance around  $940\text{ cm}^{-1}$  due to vibration between Si and O of Si–OH bond, as shown later in Fig. 3(a).<sup>20,23,26</sup> This peak and its intensity are presented as OH1 peak and  $I_{OH1}$ , respectively. The other one is an integrated area of normalized absorbance intensity from  $3000$ – $3700\text{ cm}^{-1}$ , in which O–H vibrations of Si–OH and  $H_2O$  appear, as shown later in Fig. 3(b).<sup>22,24,26</sup>

**Table I.** Abbreviation list of PDH processes with various process gases and NPdH.

Process gas	TEC + $O_3 + O_2$	$O_3 + O_2$	TEC + $O_2$	$O_2$	$N_2$	NPdH
Process name	$P_1$	$P_2$	$P_3$	$P_4$	$P_5$	$P_0$

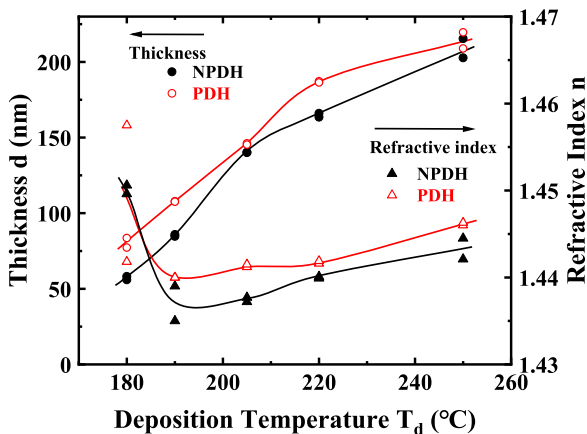
This broad peak and its integrated area are presented as OH2 peak and  $S_{OH2}$ , respectively.

### 3. Results

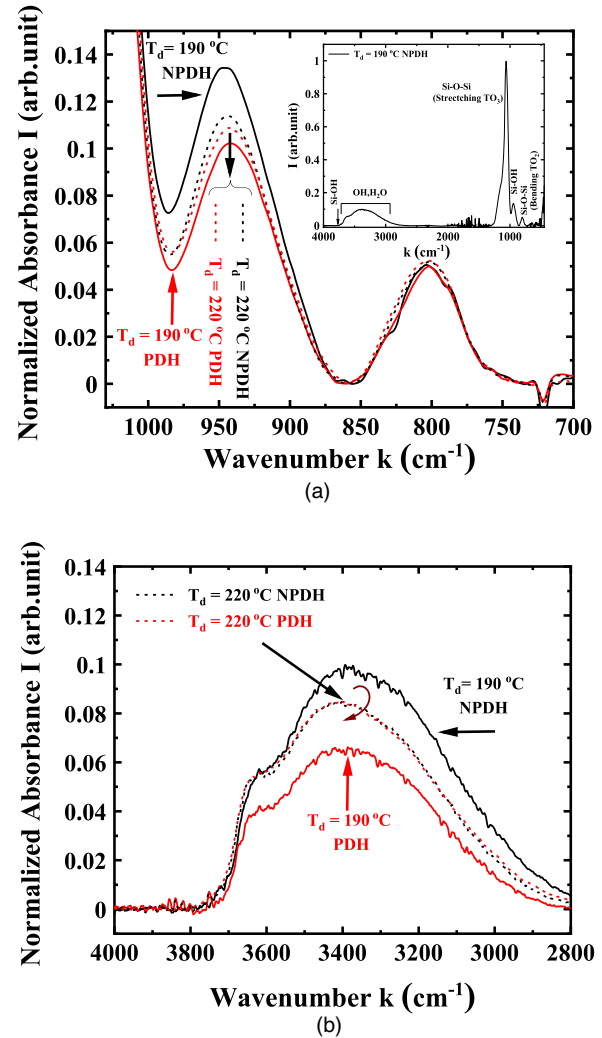
#### 3.1. Deposition temperature dependence

Figure 2 shows the deposition temperature  $T_d$  dependences of film thickness (circle)  $d$  and refractive index (triangle)  $n$  of the films deposited with the NPDH and PDH processes, where two samples were measured for each temperature. The black closed and red open plots represent NPDH and PDH, respectively. As can be seen from this figure,  $d$  increases with increasing  $T_d$ , but over  $T_d = 220$  °C, it has a tendency to saturate with  $T_d$ . This can be explained by surface and gas-phase reactions.<sup>10,27–30</sup> It is also found that the films treated by PDH are a little thicker than the NPDH case at every  $T_d$ . This is because, even after stopping the supply of SO vapor from the deposition source, a small amount of SO vapor still remains in the reaction chamber for a while. On the other hand, except for the low  $T_d$  of 180 °C, the refractive index  $n$  increases with  $T_d$  monotonically. This is because the film density increases with  $T_d$  due to the enhanced chemical reaction so that the higher film density shows the higher refractive index according to the Lorentz–Lorenz model.<sup>31,32</sup> Furthermore, it is observed that the PDH process increases  $n$  a little, compared with the NPDH case. As mentioned later, the PDH process can reduce a number of OH bonds in the deposited  $SiO_x$  films, which makes the films densify. For the larger  $n$  of the films deposited at  $T_d = 180$  °C, densification might be caused by a small amount of impurities due to insufficient chemical reaction by the reactant gas under an insufficiently high  $T_d$ , but the reason is not well understood at present.

Figures 3(a) and 3(b) show typical FT-IR spectra of the  $SiO_x$  films deposited at 190 °C (solid lines) and 220 °C (broken lines) for the NPDH (black lines) and PDH (red lines) cases, where the wavenumber ranges of (a) and (b) are 700–1030 and 2800–4000  $cm^{-1}$ , respectively. For a reference, a whole spectrum of an NPHD-treated film at 190 °C is shown in Fig. 3(a) as an inset. The peaks at  $\sim 800$  and  $940$   $cm^{-1}$  in Fig. 3(a) are identified as absorptions due to the bending of Si–O–Si bond ( $TO_2$ ) and vibration of Si–OH bond, respectively. The broad peaks in Fig. 3(b) consist of



**Fig. 2.** Deposition temperature  $T_d$  dependences of the film thickness (circle)  $d$  and refractive index (triangle)  $n$  of the films deposited by the NPDH and PDH processes. Data of two samples are plotted for each  $T_d$ . Black closed and red open shapes represent NPDH and PDH, respectively.



**Fig. 3.** Typical FT-IR spectra of the films deposited at 190 °C (solid lines) and 220 °C (broken lines) for the NPDH (black lines) and PDH (red lines) cases. Wavenumber ranges of (a) and (b) are 700–1030 and 2800–4000  $cm^{-1}$ , respectively. Inset in Fig. 3(a) shows a whole FT-IR spectrum for the NPDH at 190 °C as a reference.

overlapping vibrations due to O–H of Si–OH and  $H_2O$  bond.<sup>12,20,33</sup> For the  $T_d = 190$  °C case, it can be seen from both Figs. 3(a) and 3(b) that the OH1 peak and OH2 broad peak of the NPDH-treated film are decreased by the PDH process. This means that, with the PDH process, OH content including  $H_2O$  is reduced due to dehydration reaction of  $Si-OH + Si-OH \rightarrow Si-O-Si + H_2O \uparrow$  and evaporation of  $H_2O$ . In contrast, for the 220 °C case, the 940  $cm^{-1}$  peak decreases a little from the NPDH to the PDH, and the OH2 broad peak for the NPDH is almost the same as that for the PDH. This means that, for the  $T_d = 220$  °C case, the number of OH bonds is hardly changed by the PDH process, which will be discussed in more detail later.

Figure 4 shows the dependences of  $S_{OH2}$  (circles) and  $I_{OH1}$  (triangles) on deposition temperature  $T_d$ , where the black closed and red open shapes indicate the NPDH and PDH cases, respectively. It can be seen from this result that the  $S_{OH2}$  and  $I_{OH1}$  for the NPDH case are roughly decreased with increasing  $T_d$ , which means that increasing  $T_d$  reduces OH content due to the enhanced chemical reaction. However, for the PDH case at  $T_d \leq 220$  °C, it is very interesting that both  $S_{OH2}$  and  $I_{OH1}$  are lower than those at 220 °C, which is the

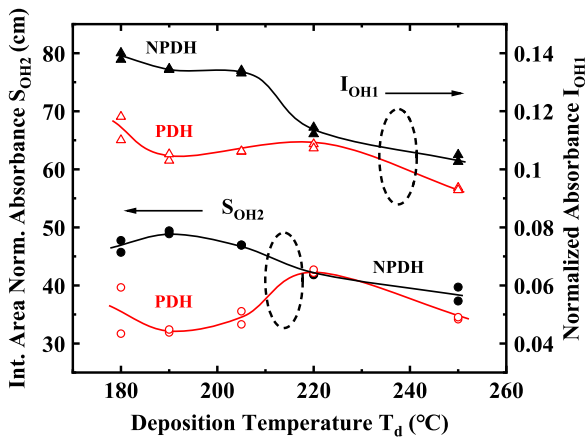


**Fig. 4.** Dependences of  $S_{OH2}$  (circles) and  $I_{OH1}$  (triangles) on the deposition temperature  $T_d$ . Black and red shapes indicate the NPDH and PDH cases, respectively.

opposite tendency to the NPDH case. This suggests that it be possible to obtain an  $SiO_x$  film with lower OH content at lower  $T_d$  if the deposition conditions are well controlled. We try to explain this as follows. It can be expected that the structure of a  $SiO_x$  film deposited at lower  $T_d$  is easily reconstructed due to weaker bond strength between Si and O atoms. In addition, the as-deposited  $SiO_x$  films at lower  $T_d$  have a greater number of OH bonds compared with the films deposited at higher  $T_d$ , as shown in Fig. 4. Therefore, during the PDH process, a substantial number of OH bonds are removed from the as-deposited  $SiO_x$  film through an active dehydration reaction between many neighbors of OH bonds, assisted by the wake chemical bonds. This leads to the collapse of numerous microspaces left after the dehydration reaction and to a concomitant rearrangement of the film structure, which makes the film densify, as mentioned previously. This easily reconstructible behavior of  $SiO_x$  film is similar to solid phase epitaxial growth of an amorphous Si film on a crystal Si substrate. It has been reported that an amorphous-phase Si film without any crystalline region can easily be crystallized on a crystal Si substrate in solid phase by annealing at a low temperature, e.g. 600 °C (mp of Si: 1410 °C), and an amorphous + crystalline mixed-phase Si film is hardly recovered to a perfect crystal Si with the remaining defects even at much higher temperature.<sup>34,35</sup> This model is in good agreement with the results of Fig. 2, which show that  $n$  of the films is increased due to the PDH process. However, by further increasing  $T_d$  to 220 °C, the structure of an as-deposited film becomes harder and contains a smaller amount of OH, both  $S_{OH2}$  and  $I_{OH1}$ , and after the PDH process are almost the same as those of the NPDH case. Furthermore, by increasing  $T_d$  to 250 °C the chemical dehydration reaction becomes more active due to higher thermal energy so that the OH content can be further reduced by the 5 min PDH process from the NPDH case.

Indeed, the structural change of a deposited  $SiO_x$  film can be seen by observing the shift of the peak position and shape of the  $TO_3$  mode in the FT-IR spectrum. It is known that wavenumber  $k_p$  of a peak position of the  $TO_3$  mode can be approximated by an expression of the form,  $k_p = k_0 \sin(\theta/2)$ , where  $k_0$  is a constant depending on the mass of the O atom and the force constant between O and Si, and  $\theta$  is the Si–O–Si

bridging bond angle.<sup>36,37</sup> Assuming that  $k_0$  is invariant for any deposition condition, a positive or negative shift of  $k$  from a standard peak position indicates a positive or negative change in  $\theta$  from the standard bonding angle. The width of the peak can also be understood in terms of a statistical distribution of  $\theta$  and summation over narrow angles. Therefore, a change in the  $k_p$  and peak form can be regarded as a change of  $SiO_x$  film structure. Figure 5 shows the  $T_d$  dependences of wavenumbers of the peak position  $k_p$ , the 1st derivative maximum  $k_{pdmax}$  and the 1st derivative minimum  $k_{pdmin}$  of the  $TO_3$  mode peak. Since the  $TO_3$  mode peak is unsymmetric, the  $k_{pdmin}$  and  $k_{pdmax}$  positions are also unsymmetric with respect to  $k_p$ , which means that  $(k_{pdmin} - k_p)$  is different to  $(k_p - k_{pdmax})$ . As can be seen from Fig. 5, at  $T_d \leq 205$  °C, the characteristic  $k$  values for the PDH case (red lines) are obviously higher than those for the NPDH case (black lines). These results indicates that the film structures were clearly changed by the PDH treatment at  $T_d \leq 205$  °C. Consequently, it can also be deduced that the structures of the  $SiO_x$  films deposited at  $T_d \leq 205$  °C are easily reconstructible compared with that at higher  $T_d$ .

By means of the preservation of as-deposited  $SiO_x$  films, we investigated the PDH effect on the remaining OH content in the preserved films. The tested samples were  $SiO_x$  films deposited at 190 °C and 220 °C, which are the most and the least effective for the reduction of OH content by the PDH process, respectively, as shown in Fig. 4. Figures 6(a) and 6(b) show the typical FT-IR spectra of the  $SiO_x$  films deposited at 190 °C and 220 °C, respectively, where the wavenumber range is 2800–4000  $cm^{-1}$ . In each figure, the two films are just as deposited without PDH (NPDH, black) and with PDH (red), and the other two films deposited without PDH (NPDH, blue) and with PDH (green) were preserved for 12 h in dry air.

For the films at  $T_d = 190$  °C of Fig. 6(a), the OH content of the NPDH-treated and preserved film (blue) is reduced without heating from that of the as-deposited and NPDH-treated one (black), but with a smaller reduction level than that of the PDH-treated films. This reduction is due to self-dehydration reaction in the film even at RT after deposition since the film structure is easily reconstructible at  $T_d = 190$  °C. On the other hand, for the two films treated by the PDH process (red and green lines), the spectral shapes

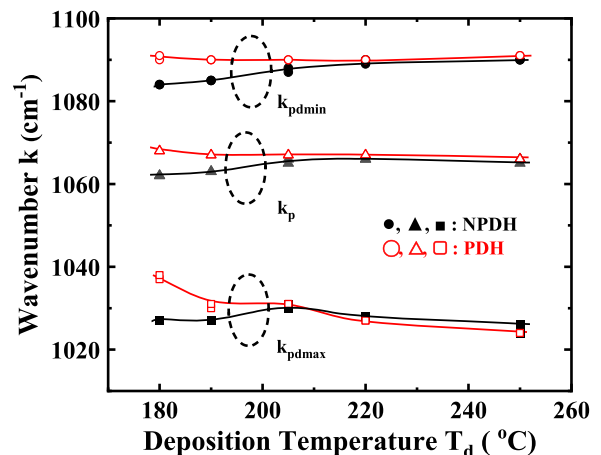


**Fig. 5.** Deposition temperature  $T_d$  dependences of the wavenumbers of the peak position  $k_p$ , the 1st derivative maximum  $k_{pdmax}$  and the 1st derivative minimum  $k_{pdmin}$  of the  $TO_3$  mode peak.

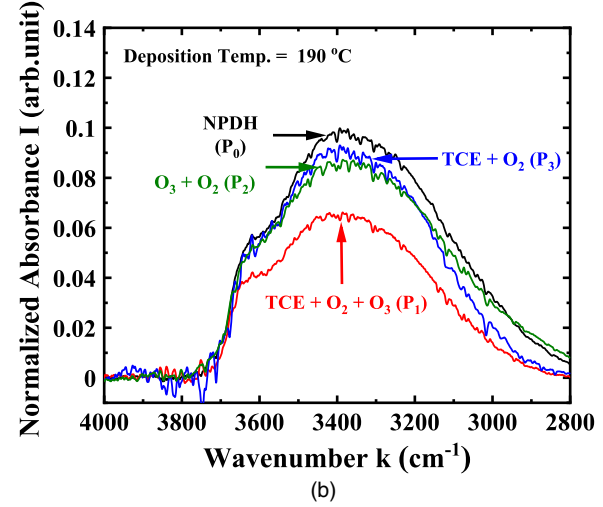
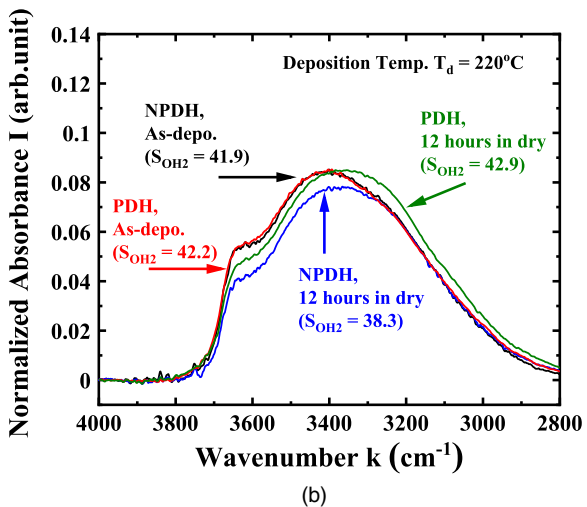
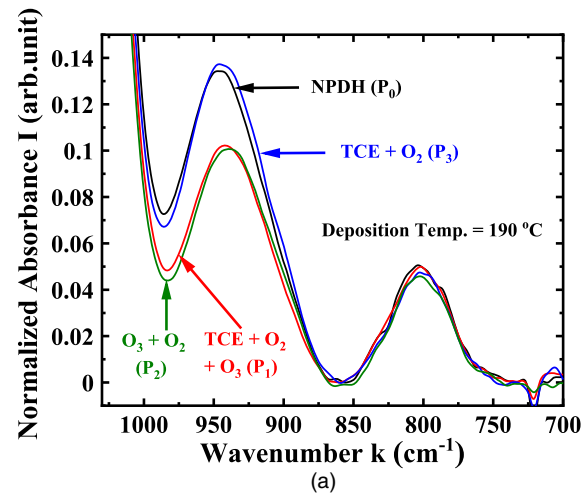
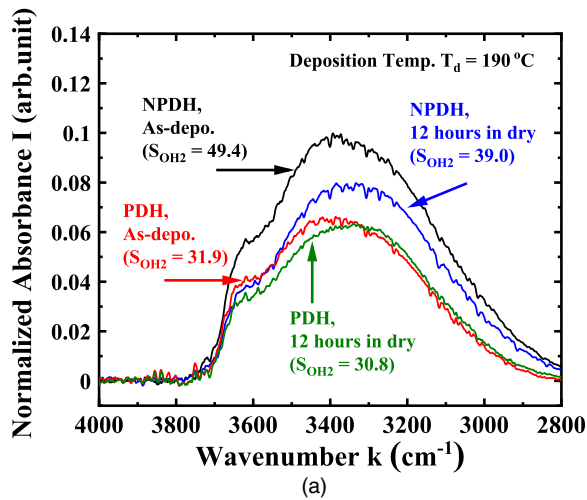


**Fig. 6.** Typical FT-IR spectra of the SiO<sub>x</sub> films deposited at (a) 190 °C and (b) 220 °C in the wavenumber range of 2800–4000 cm<sup>-1</sup>. Black and red lines represent only as-deposited films with the NPdH and PDH processes, respectively. Blue and green lines represent the preserved films treated by the NPdH and PDH processes, respectively.

**Fig. 7.** Typical FT-IR spectra of the SiO<sub>x</sub> films PDH-treated at 190 °C with the various conditions of the process gas. Wavenumber ranges of (a) and (b) are 700–1030 and 2800–4000 cm<sup>-1</sup>, respectively. Process gas conditions are P<sub>1</sub> (red line), P<sub>2</sub> (green line) and P<sub>3</sub> (blue line). As a reference, P<sub>0</sub> (black line) of NPdH is shown.

are almost the same, although a small difference can be seen between them in the higher wavenumber range of 3400–3700 cm<sup>-1</sup>. This means that the PDH-treated SiO<sub>x</sub> films are more stable than the ones without the PDH process. In contrast, for the 220 °C-deposition case of Fig. 6(b), the difference in spectral shape is not as large as that in the 190 °C case of Fig. 6(a) regardless of preservation and the PDH process. However, every S<sub>OH2</sub> (38 ~ 43) at 220 °C is larger than those (30 ~ 32) of the PDH case at 190 °C, as shown in Fig. 6(b). This means that the PDH process at lower T<sub>d</sub> = 190 °C is useful and effective not only for reduction of OH content, but also suppression of increment of OH content in preservation. In addition, it can be considered from this result that the structure-changed film due to the PDH process is relatively denser so that moisture or the source of OH bonds might hardly be diffused into the film.

### 3.2. Dependence on process gas in PDH

Figures 7(a) and 7(b) show typical FT-IR spectra of the SiO<sub>x</sub> films deposited and PDH-treated at 190 °C with the various conditions of a process gas, where the wavenumber ranges of (a) and (b) are 700–1030 and 2800–4000 cm<sup>-1</sup>, respectively. Among the five kinds of PDH processes, P<sub>1</sub> (red line), P<sub>2</sub>

(green line) and P<sub>3</sub> (blue line) are selected. In addition, spectra of P<sub>0</sub> (black line) are shown as a reference. From Fig. 7(a), it can be clearly seen that the OH1 peaks for P<sub>1</sub> and P<sub>2</sub> are almost the same, and that those for P<sub>3</sub> and P<sub>0</sub> are also almost the same but much higher than the former ones. On the other hand, in Fig. 7(b), the tendency of normalized absorbance *I* is a little different to that of Fig. 7(a). While *I* of P<sub>0</sub> and P<sub>3</sub> [*I*(P<sub>0</sub>) and *I*(P<sub>3</sub>)] are almost the same as in Fig. 7(a), *I*(P<sub>1</sub>) is much lower than *I*(P<sub>2</sub>) in Fig. 7(b), which is obviously different to the Fig. 7(a) case of *I*(P<sub>1</sub>) ≈ *I*(P<sub>2</sub>).

A comparison of S<sub>OH2</sub> and I<sub>OH1</sub> in the respective PDH processes is shown as a histogram in Fig. 8 with the NPdH case as a reference, where the light blue and the hatched red bars indicate S<sub>OH2</sub> and I<sub>OH1</sub>, respectively. For each process gas condition, the bar height is the average of the two samples' data, and the difference between them is presented as a short line or error bar. It can be clearly seen that the process gas of P<sub>1</sub> is the most effective for the reduction of OH content due to the lowest S<sub>OH2</sub> and much lower I<sub>OH1</sub>. The P<sub>2</sub> process gas is also effective for the lowest I<sub>OH1</sub>, but it is not as good due to the relatively high S<sub>OH2</sub> compared with that of P<sub>1</sub>. From the viewpoint of I<sub>OH1</sub> attributed to vibration between Si and OH (Si–OH), it can be considered that O<sub>3</sub>

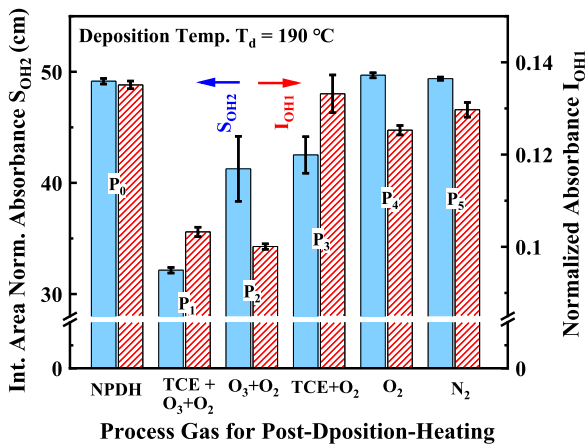


**Fig. 8.** Comparison of  $S_{OH2}$  (light blue) and  $I_{OH1}$  (hatched red) in the respective PDH processes with the NPDH case as a reference. For each bar, the average data of two samples are shown and the differences between them are presented as short lines or error bars.

plays a very important role in the reduction of OH bonds since the  $I_{OH1}$  of  $P_1$  and  $P_2$  are much smaller than those of the other processes including  $P_0$ . This is probably due to the fact that  $O_3$  assists the dehydration reaction of  $Si-OH + Si-OH \rightarrow Si-O-Si + H_2O$ , where  $O_3$  acts as a catalyst. The dehydration in  $P_2$  also leads to structural change and densification of  $SiO_x$  films such as  $P_1$ , as shown previously. Table II shows the characteristic wavenumbers in a peak of the  $TO_3$  mode for respective  $P_i$  processes such as those in Fig. 5. As can be seen,  $k_p$ ,  $k_{pdmin}$  and  $k_{pdmax}$  in  $P_2$  as well as  $P_1$  are significantly larger than those of the other processes.

Although it seems that the data of the other processes of  $P_3$ (TCE +  $O_2$ ),  $P_4$ ( $O_2$ ) and  $P_5$ ( $N_2$ ) are roughly similar to those of  $P_0$ (NPDH), a few interesting and curious points can be found when carefully comparing all the data. For example,  $I_{OH1}$  of  $P_2$  is much smaller than that of  $P_3$  but their  $S_{OH2}$  are almost the same. These discrepancies will be discussed in the next section.

#### 4. Discussion

It can be seen from Fig. 4 that the  $S_{OH2}$  behavior is almost similar to  $I_{OH1}$  probably because the signal source for both is the Si-OH bond, i.e.  $S_{OH2}$  is due to O-H vibration of Si-OH, and  $I_{OH1}$  is due to Si-OH vibration. Figure 9 shows the relationship between  $S_{OH2}$  and  $I_{OH1}$  in this study. In this figure, the black closed and red open circles represent the data for the NPDH- and PDH-treated  $SiO_x$  films, respectively. The data are used in Fig. 4, and the blue open triangles represent the films treated by the  $P_i$  processes with various gases, whose data are used in Fig. 8 except for  $P_0$  and  $P_1$ . The black broken and red one-point-broken linear lines indicate the roughly proportional relationship between  $S_{OH2}$  and  $I_{OH1}$ , where the two lines pass through the origin, which is shown

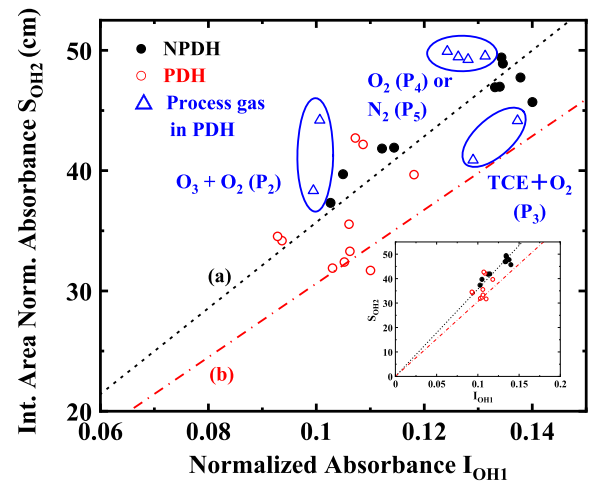


**Fig. 9.** Relationship between  $S_{OH2}$  and  $I_{OH1}$  for the NPDH- (black closed circle) and the normal PDH- (red open circle) treated  $SiO_x$  films shown in Fig. 3, and for the PDH-treated films with the various process gases  $P_i$  (blue open triangle) shown in Fig. 8 except for  $P_0$  and  $P_1$ . Black broken (a) and red one-point-broken (b) linear lines represent roughly proportional relations between  $S_{OH2}$  and  $I_{OH1}$ , i.e.  $S_{OH2} \approx C \cdot I_{OH1}$ .  $C$  of (a) is larger than that of (b) due to a larger amount of  $H_2O$  adsorption on an  $SiO_x$  film. Details are mentioned in Sect. 4. Discussion.

in the inset. Thus, the relationship can be expressed as,

$$S_{OH2} \approx C \cdot I_{OH1}, \tag{2}$$

where  $C$  is a proportional constant. The black line labeled (a) mainly corresponds to the NPDH data, and the red one labeled (b) mainly to the  $P_1$  data with the lower  $S_{OH2}$ . In this case,  $C$  for the NPDH and PDH are  $C_a = 357$  and  $C_b = 306$ , respectively. Here, we should note that the measured  $I_{OH1}$  is larger, within  $\sim 20\%$  of a true  $I_{OH1}$  of the OH1 peak because the measured one is overlapped with a small tail or shoulder of the  $TO_3$  mode peak on the lower  $k$  side, as shown in Fig. 3(a). However, this overestimation is not an essential issue in physics because it just brings a small error or fluctuation to the proportional constant “ $C$ ”, which are somewhat comparable to the scattered data of the NPDH and PDH cases. Later, we will discuss constant “ $C$ ” more deeply.

Figure 10 shows a typical FT-IR spectrum in the wavenumber range of  $2800-4000 \text{ cm}^{-1}$  with schematic pictures of four possible forms of the silanol (Si-OH) group.<sup>21,33</sup> It is well known that low-temperature deposited  $SiO_x$  films contain numerous OH bonds of the silanol group and an amount of water or moisture  $H_2O$ .<sup>(3-5,8,12,14,15)</sup> Therefore, the silanol groups are perturbed by the H bond action (“- - -”) as in the schematic picture in Fig. 10. Type (a) is an isolated silanol free of H bond, and its O-H stretching mode is responsible for a distinct sharp band at  $\sim 3740 \text{ cm}^{-1}$ . (b) is a silanol perturbed at the O atom, (c) is at the H atom, and (d) is at both atoms. In (c) and (d), H bonds are formed between

**Table II.** Wavenumbers ( $\text{cm}^{-1}$ ) at the peak position  $k_p$ , the 1st derivative minimum  $k_{pdmin}$ , the 1st derivative maximum  $k_{pdmax}$  of the  $TO_3$  mode peak for each PDH process. As a reference, the NPDH data are shown. The values are averages of two samples under the same process gas condition.

Gas process	TEC + $O_3$ + $O_2$ $P_1$	$O_3$ + $O_2$ $P_2$	TEC + $O_2$ $P_3$	$O_2$ $P_4$	$N_2$ $P_5$	NPDH $P_0$
$k_{pdmin}$	1090	1090	1086	1086	1086	1085
$k_p$	1067	1067	1064	1064	1064	1063
$k_{pdmax}$	1031	1033	1030	1029	1028	1027

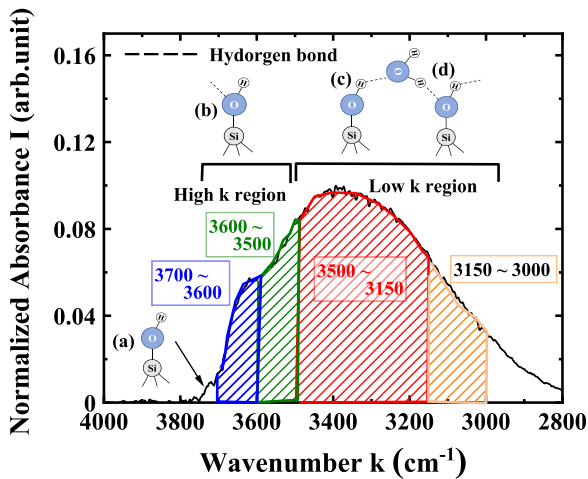


**Fig. 10.** Typical FT-IR spectrum in the wavenumber range of 2800–4000  $\text{cm}^{-1}$  with schematic pictures of four possible forms of the silanol (Si–OH) group. Range of wavenumber  $k$  is divided into the four regions according to the degree of affect of H bond on silanol.

silanols and one  $\text{H}_2\text{O}$  molecule. Since H bond affects silanol more strongly, absorption wavenumber  $k$  is shifted lower. In other words, when the H bond further weakens the atomic bond strength of O–H in silanol, wavenumber  $k$  is further lowered. Here, we divide the range of measurement wavenumber  $k$  into four regions, 3700–3600, 3600–3500, 3500–3150, and 3150–3000  $\text{cm}^{-1}$ . Figure 11 shows the relationship between the four divided  $k$  regions and the ratios in  $S_{\text{OH}2}$  of PDH/NHP as a function of the deposition temperature  $T_d$ , where the data for 180, 190, 205, 220, and 250  $^\circ\text{C}$  are indicated by black triangle, red circle, blue square, green diamond and pink star shapes, respectively. Each data plot is an average of two samples under the same condition. A lower ratio means a larger reduction in OH content by the PDH process. It can be seen from this figure that the PDH effect on the reduction of  $S_{\text{OH}2}$  is stronger in the lower  $k$  region at any  $T_d$  except for  $T_d = 220^\circ\text{C}$ . The exception of 220  $^\circ\text{C}$  can be expected based on the results of Fig. 4. Consequently, the

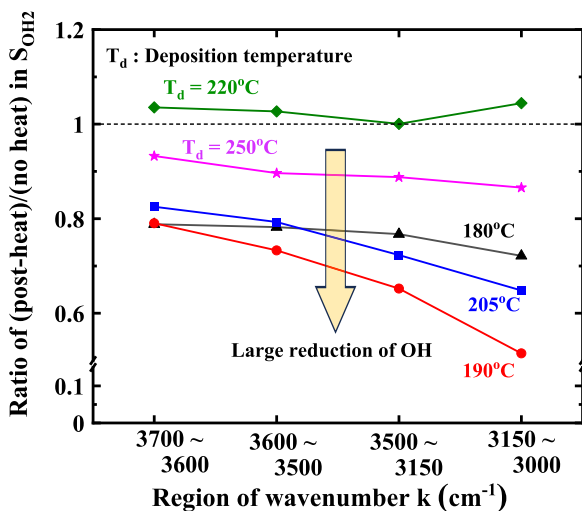


**Fig. 11.** Relationship between the four divided  $k$  regions and the ratios in  $S_{\text{OH}2}$  of PDH/NPDH as a function of deposition temperature  $T_d$ . Data for 180, 190, 205, 220, and 250  $^\circ\text{C}$  are indicated by black triangle, red circle, blue square, green diamond and pink star shapes, respectively. Each data plot is an average of two samples under the same conditions.

dehydration reaction between OH bonds is further promoted by the stronger effect of the H bond so that Si–OH bonds of the silanol group vanish more easily.

Based on the above discussion, we will further discuss a few questions raised by Fig. 8. Question 1 (Q1): why is the  $S_{\text{OH}2}$  of  $P_2$  relatively higher despite its lowest  $I_{\text{OH}1}$ ? Q2: why is the  $I_{\text{OH}1}$  of  $P_3$  much larger than that of  $P_2$ , although both  $S_{\text{OH}2}$  are nearly equal? Q3: why are the error bars of  $P_2$  and  $P_3$  larger compared with the other ones? Finally, Q4: why are the  $S_{\text{OH}2}$  of  $P_4(\text{O}_2)$  and  $P_5(\text{N}_2)$  still higher after the PDH process while their  $I_{\text{OH}1}$  are slightly reduced? It is hard to consider that these questions come from faults in measurement and deposition because they have good reproducibility. In order to gain some insight into the answers to these questions, we take the difference in FT-IR spectrum between the  $P_i$  processes, as shown in Fig. 12, where the black, blue, and red lines represent the FT-IR spectra of  $(P_0 - P_1)$ ,  $(P_2 - P_1)$  and the  $(P_2 - P_3)$ , respectively. It can be seen from this figure that  $(P_0 - P_1)$  is larger as a whole, compared to  $(P_2 - P_1)$  and  $(P_2 - P_3)$ . In addition, the shape of the blue  $(P_2 - P_1)$  is round and broad, whereas that of the red  $(P_2 - P_3)$ , by contrast, is wavy with negative and positive split regions. As shown in Figs. 10 and 11, the H bond effect on silanol is stronger in the lower region of  $k$ , which is roughly related to the number of OH bonds and  $\text{H}_2\text{O}$ . Furthermore,  $\text{H}_2\text{O}$  or moisture comes from not only the deposition reaction, but also from adsorption on the surface of  $\text{SiO}_x$  films through the PDH process and the deposited films being exposed to air.

Taking the above insight and the results of Fig. 12 into account, we try to answer the aforementioned questions Q1 to Q4 as follows. If the amount of  $\text{H}_2\text{O}$  adsorption is assumed to depend on number of Si–OH bonds or  $I_{\text{OH}1}$ , the proportional constant “C” of Eq. 2 is caused by O–H vibrations of not only Si–OH, but also  $\text{H}_2\text{O}$ , as shown in Fig. 13. Thus, we can express C as  $C = C_{\text{Si-OH}} + C_{\text{H}_2\text{O}}$ , where  $C_{\text{Si-OH}}$  and  $C_{\text{H}_2\text{O}}$  are attributed to Si–OH and  $\text{H}_2\text{O}$ , respectively. Therefore, the difference in  $I$  of  $(P_2 - P_1)$  in Fig. 12 may be due to the difference in the amount of adsorbed  $\text{H}_2\text{O}$  on the sample or  $C_{\text{H}_2\text{O}}$ . This can be the answer to Q1. In fact, the plots of  $P_2$  in Fig. 9 are above the broken (a) line. Likewise, we can answer Q2. Since the two  $P_3$  plots are within the two (a) and (b) lines in Fig. 9, the  $C_{\text{H}_2\text{O}}$  for  $P_3$  should be smaller than that for  $P_2$ , which means that the ratio amount of adsorbed  $\text{H}_2\text{O}$  and silanol for  $P_3$ ,  $C_{\text{H}_2\text{O}}/C_{\text{Si-OH}}$ , is smaller than

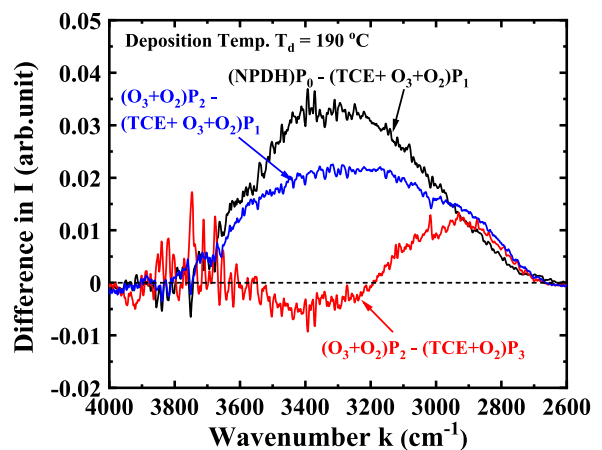


**Fig. 12.** Difference in FT-IR spectra of  $(P_0 - P_1)$  (black),  $(P_2 - P_1)$  (blue) and  $(P_2 - P_3)$  (red).  $P_i$  is a PDH process abbreviation with one kind of process gas and the detail is given in Table I.



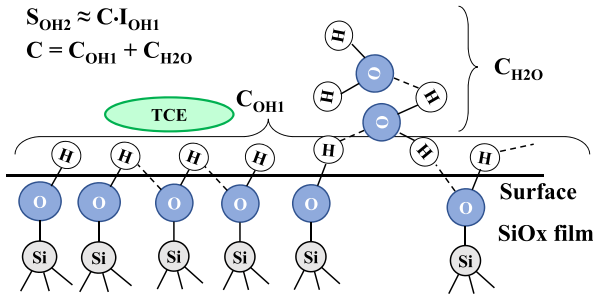


**Fig. 13.** Schematic model to explain the relationship between  $S_{OH2}$  and  $I_{OH1}$  shown in Fig. 9.  $S_{OH2}$  can be expressed as  $S_{OH2} \approx C \cdot I_{OH1}$ , where  $C$  is a proportional constant and is attributed to two factors of  $C_{Si-OH}$  and  $C_{H2O}$ , where  $C_{Si-OH}$  and  $C_{H2O}$  originate from Si-OH and H<sub>2</sub>O, respectively.

that for P<sub>2</sub>. Furthermore, we can explain why the H<sub>2</sub>O adsorption constant  $C_{H2O}$  for P<sub>2</sub> is larger than those for P<sub>1</sub> and P<sub>3</sub>. As shown in Fig. 13, an amount of hydrophobic TCE, which is a PDH process gas, probably adsorbs and remains on the surface of the deposited SiO<sub>x</sub> film in the P<sub>1</sub> and P<sub>3</sub> cases. Thus, the adsorption of hydrophilic H<sub>2</sub>O from the atmosphere may be prevented on the TCE-adsorbed surface. In contrast, H<sub>2</sub>O adsorption in the P<sub>2</sub> case can easily occur on a surface almost without TCE. This small amount of TCE on the surface results from there being no TCE supply and the removal of TCE that remains on the surface due to chemically reactive O<sub>3</sub> during the PDH process. The explanation with TCE adsorption can also be applied to an answer for Q3 in respect of the relatively larger error bars in  $S_{OH2}$  of the P<sub>2</sub> and P<sub>3</sub> cases. This is because the degree or amount of TCE adsorption on the surface of a deposited oxide film is somehow uncertain and difficult to strictly control. In addition, covering the film surface with TCE might influence the  $I_{OH1}$  value of P<sub>3</sub> since the error bar of  $I_{OH1}$  is large. Finally, we discuss Q4, i.e., the reason why the  $I_{OH1}$  of P<sub>4</sub> and P<sub>5</sub> are a little smaller than that of the NPDH while the  $I_{OH1}$  of P<sub>3</sub>, in which only TCE is added to P<sub>4</sub>, is at the same level as the NPDH. The small reduction in  $I_{OH1}$  for P<sub>4</sub> and P<sub>5</sub> can be explained by the so-called annealing effect through the 5 min PDH process. However, for the  $I_{OH1}$  of P<sub>3</sub>, we still do not have a clear answer, although there is the possibility that TCE might somehow prevent the annealing effect.

We have discussed the Q1 to Q4 questions, as mentioned above, and explained the answers. However, some unanswered questions still remain because we do not know enough about the detailed mechanisms of SiO<sub>x</sub> film growth at present. Consequently, further discussion and investigation is necessary.

### 5. Conclusion

In this study, we investigated the PDH effect on OH content in the SiO<sub>x</sub> films deposited by APCVD using the deposition source of SO with the reactive gas of O<sub>3</sub> and TCE vapor at the temperature  $T_d$  of 180 °C–250 °C. The PDH process is performed in situ for 5 min without any supply of SO in the deposition chamber just after film deposition, where the heating temperature is the same as  $T_d$ . While OH content in the films without the PDH process or with the NPDH process decreased with increasing  $T_d$  due to thermal-energy-enhanced chemical reaction, those with the PDH process decrease with decreasing  $T_d$  from 220 °C. At  $T_d = 190$  °C, the minimum OH content in the SiO<sub>x</sub> film can be obtained. This PDH effect on

OH reduction can be considered due to the easily reconstructible structure of SiO<sub>x</sub> films deposited at lower  $T_d$ . This reconstructible structure probably results from weaker bond strength between Si and O atoms and is promoted by the large number of OH bonds in SiO<sub>x</sub> film deposited at lower  $T_d$ , where a substantial amount of the OH bonds are removed by dehydration reaction in the PDH process. This is a curious point for the low-temperature deposition of SiO<sub>x</sub> film because lower OH content can be obtained at lower temperature in the case of limited  $T_d \leq 200$  °C. Furthermore, we found one key process gas for the reduction of OH content in the PDH process. This is O<sub>3</sub>, which acts as a catalyst for the reduction of OH bonds. For TCE, it plays the role of suppression of H<sub>2</sub>O adsorption on an as-deposited SiO<sub>x</sub> film, in particular, air exposure of a film probably due to its hydrophobic property. However, it may have no effect on the reduction of OH content in deposited SiO<sub>x</sub> films after deposition.

### Acknowledgment

This research is partially supported by JSPS KAKENHI, Grant No. JS21K04649.

### Appendix

Assuming that the peak form is a Gaussian curve, the peak intensity  $I$  as a function of  $k$  is expressed by,

$$I(k) = \exp\left(-\frac{k^2}{2W^2}\right), \text{ where } I(0) = 1. \quad (\text{A-1})$$

Then, the 1st derivative and the 2nd derivative of Eq. (A-1) are calculated as,

$$I'(k) = -\frac{k}{W^2} \exp\left(-\frac{k^2}{2W^2}\right), \quad (\text{A-2})$$

and

$$I''(k) = \frac{1}{W^2} \left(\frac{k^2 - W^2}{W^2}\right) \exp\left(-\frac{k^2}{2W^2}\right). \quad (\text{A-3})$$

Therefore,  $k$  values at the negative minimum of  $I'(k)$ ,  $k_{dmin}$ , and the positive maximum,  $k_{dmax}$ , are  $W$  and  $-W$ , respectively. Because FWHM of  $I(k)$  is calculated to be  $2\sqrt{\ln(2)}W$ , the FWHM is proportional to  $k_{dmin} - k_{dmax} = 2W$ .

- 1) S. Higashi, D. Abe, S. Inoue, and T. Shimoda, *Jpn. J. Appl. Phys.* **40**, 4171 (2001).
- 2) M. M. Moslehi, R. A. Chapman, M. Wong, A. Paranjpe, H. N. Najm, J. Kuehne, R. L. Yeakley, and C. J. Davis, *IEEE Trans. Electron Devices* **39**, 4 (1992).
- 3) T. Kawahara, A. Yuuki, and Y. Matsui, *Jpn. J. Appl. Phys.* **31**, 2925 (1992).
- 4) N. Hirashita, S. Tokitoh, and H. Uchida, *Jpn. J. Appl. Phys.* **32**, 1787 (1993).
- 5) A. M. Mahajan, L. S. Patil, J. P. Bange, and D. K. Gautam, *Vacuum* **79**, 194 (2005).
- 6) G. Mannino, R. Ruggeri, A. Alberti, V. Privitera, G. Fortunato, and L. Maiolo, *Appl. Phys. Express* **5**, 021103 (2012).
- 7) T. Toriyabe, K. Nishioka, and S. Horita, Proc. 13th Int. Display Workshops (IDW'06), 2006, p. 719.
- 8) S. Horita, K. Toriyabe, and K. Nishioka, *Jpn. J. Appl. Phys.* **48**, 035502 (2009).
- 9) H. Nakashima, K. Omae, T. Takebayashi, C. Ishizuka, and T. Uemura, *J. Occup. Health* **40**, 270 (1998).
- 10) S. Horita and P. Jain, *Jpn. J. Appl. Phys.* **56**, 088003 (2017).
- 11) P. Jain and S. Horita, Proc. 21st Int. Workshop Active-Matrix Flatpanel Displays and Devices (AM-FPD), 2017, p. 285.
- 12) S. Horita and P. Jain, *Jpn. J. Appl. Phys.* **57**, 03DA02 (2018).

- 13) J. McMurry, *Fundamentals of Organic Chemistry* (Brooks/Cole, Belmont, CA, 2011) 7th ed., p. 339.
- 14) M. Matsuura, Y. Hayashide, H. Kotani, and H. Abe, *Jpn. J. Appl. Phys.* **30**, 1530 (1991).
- 15) Y. Nishi, T. Funai, H. Izawa, T. Fujimoto, H. Morimoto, and M. Ishii, *Jpn. J. Appl. Phys.* **31**, 4570 (1992).
- 16) T. Ito, T. Matumoto, and K. Nishioka, *Surf. Coat. Technol.* **215**, 447 (2013).
- 17) S. S. Kim, D. J. Stephens, G. Lucovsky, G. G. Fountain, and R. J. Markunas, *J. Vac. Sci. Technol. A* **8**, 2039 (1990).
- 18) L. C. D. Goncalves, C. E. Viana, J. C. Santos, and N. I. Morimoto, *Surf. Coat. Technol.* **180–181**, 275 (2004).
- 19) S. Horita and D. Pu, Abstr. 9th Int. Symp. Organic and Inorganic Electronic Materials and Related Nanotechnologies, 2023, p. 283, EM-NANO 2023.
- 20) J. A. Theil, D. V. Tsu, M. W. Watkins, S. S. Kim, and G. Lucovsky, *J. Vac. Sci. Technol. A* **8**, 1374 (1990).
- 21) H. Rinnert and M. Vergnat, *J. Non-Cryst. Solids* **320**, 64 (2003).
- 22) P. Lange, U. Schnakenberg, S. Ullerich, and H.-J. Schliwinski, *J. Appl. Phys.* **68**, 3532 (1990).
- 23) A. Barranco, F. Yubero, J. Cotrino, J. P. Espinós, J. Benítez, T. C. Rojas, J. Allain, T. Girardeau, J. P. Rivière, and A. R. González-Elipe, *Thin Solid Films* **396**, 9 (2001).
- 24) P. Innocenzi, P. Falcaro, D. Grosso, and F. Babonneau, *J. Phys. Chem. B* **107**, 4711 (2003).
- 25) A. Savitzky and M. J. E. Golay, *Anal. Chem.* **36**, 1627 (1964).
- 26) R. M. Almeida and C. G. Pantano, *J. Appl. Phys.* **68**, 4225 (1990).
- 27) K. Fujino, Y. Nishimoto, N. Tokumasu, and K. Maeda, *J. Electrochem. Soc.* **137**, 2883 (1990).
- 28) Y. Ikeda, Y. Numasawa, and M. Sakamoto, *J. Electron. Mater.* **19**, 45 (1990).
- 29) E. J. Kim and W. N. Will, *J. Cryst. Growth* **140**, 315 (1994).
- 30) M. Ouyang, C. Yuan, R. J. Muisener, A. Boulares, and J. T. Koberstein, *Chem. Mater.* **12**, 1591 (2000).
- 31) L. Bányai and P. Gartner, *Phys. Rev. B* **29**, 728 (1984).
- 32) K. E. Oughstun and N. A. Cartwright, *Opt. Express* **11**, 1541 (2003).
- 33) A. Fidalgo and L. M. Ilharco, *J. Non-Cryst. Solids* **283**, 144 (2001).
- 34) M. Miyao, N. Yoshihiro, T. Tokuyama, and T. Mitsuishi, *J. Appl. Phys.* **50**, 223 (1979).
- 35) H. Ishiwara and S. Horita, *Jpn. J. Appl. Phys.* **24**, 568 (1985).
- 36) G. Lucovsky, M. J. Manitini, J. K. Srivastava, and E. A. Irene, *J. Vac. Sci. Technol. B* **5**, 530 (1987).
- 37) J. T. Fitch, G. Lucovsky, E. Kobeda, and E. A. Irene, *J. Vac. Sci. Technol. B* **7**, 153 (1989).